Research Article

Cancer Prevention Research

Sarsaparilla (*Smilax Glabra* Rhizome) Extract Inhibits Cancer Cell Growth by S Phase Arrest, Apoptosis, and Autophagy via Redox-Dependent ERK1/2 Pathway

Tiantian She[1], Like Qu[1], Lixin Wang[1], Xingxin Yang[2], Shuo Xu[3], Junnan Feng[1], Yujing Gao[4], Chuanke Zhao[1], Yong Han[1], Shaoqing Cai[2], and Chengchao Shou[1]

Abstract

Cancer is still the major cause of death across the world. Regular approaches cannot effectively solve the emerging problems, including drug/radiation resistance, side effects, and therapeutic ineffectiveness. Natural dietary supplements have shown effectiveness in the prevention and treatment of cancer. Sarsaparilla (*Smilax Glabra* Rhizome) has growth-inhibitory effects on several cancer cell lines *in vitro* and *in vivo*, with little toxicity on normal cells. However, the mechanism underlying its function remains elusive. In the present study, we examined the anticancer activity of the supernatant of the water-soluble extract (SW) from sarsaparilla. Liquid chromatography/mass spectrometry–ion trap–time-of-flight (LC/MS-IT-TOF) analysis identified flavonoids, alkaloids, and phenylpropanoids as the major bioactive components of SW. SW was shown to markedly inhibit the growth of a broad spectrum of cancer cell lines in the *in vitro* and *in vivo* assays. S phase arrest, autophagy, or/and apoptosis were partly responsible for SW-induced growth inhibition. Results of microarray analysis and validation by quantitative RT-PCR indicated the involvement of oxidative stress and the MAPK1 pathway in SW-treated cells. We further found that SW destroyed intracellular-reduced glutathione/oxidized glutathione (GSH/GSSG) balance, and supplement with N-acetylcysteine (NAC) or glutathione (GSH) significantly antagonized SW-induced S phase arrest, apoptosis, and autophagy. In addition, SW-induced GSH/GSSG imbalance activated the ERK1/2 pathway, which contributed to SW-induced S phase arrest, apoptosis, autophagy, and resultant growth-inhibitory effect. Together, our results provide a molecular basis for sarsaparilla as an anticancer agent. *Cancer Prev Res; 8(5); 464–74.* ©*2015 AACR.*

Introduction

Cancer, with ever-growing incidence and mortality, threatens human health and quality of life worldwide. By 2030, there would be an estimated increment of 20.3 million new cases, with 13.2 million cancer-related deaths (1); therefore, both preventive and therapeutic approaches are critical for the fight against cancer. Natural dietary supplements, belonging to Nutritional Therapeutics of Complementary and Alternative Medicine field, provide a practical choice for cancer prevention and treatment (2–6).

Sarsaparilla, also known as *Smilax Glabra* Rhizome (SGR) or *Smilax Glabra* Roxb (7, 8), regularly serves as a supplement of herbal formula in treating diseases such as syphilis, gout, gonorrhea, inflammation, liver problems, and cancer in Southeast Asia and North America (9–11). Several reports revealed the roles of sarsaparilla in modulating immunity (12), protecting liver from injuries (13), lowering blood glucose level (14), and inhibiting cancer development (15); however, there is no epidemiologic evidence regarding sarsaparilla's functions.

Sarsaparilla extract showed killing effect on WiDr (human colon cancer cell), HeLa, and human leukemia cells, with little cytotoxicity to human umbilical vein enduothelial cells (10, 16). Herbal formula containing sarsaparilla restrained xenograft growth in mice and ameliorated the condition of patients with middle or late-stage primary hepatic carcinoma (15, 17). Our previous study demonstrated the anticancer effect of total ethanol extract of sarsaparilla *in vitro* and *in vivo*, which correlated with activation of the mitochondrial apoptotic pathway (7). S or S–G_2 phase arrest was also attributed to sarsaparilla's function (18). However, the exact mechanism underlying sarsaparilla's inhibitory effects on cancer cell growth remains obscure.

To evaluate the biologic effect of sarsaparilla, several means of extraction had been developed (7, 10, 16, 18). In the present study, we optimized extraction procedures and sequentially separated the total ethanol extract of sarsaparilla into six fractions. Results of *in vitro* screening assay revealed that the supernatant of water-soluble fraction (SW) possessed strongest anticancer potential, and mass spectrometry analysis identified major

[1]Key Laboratory of Carcinogenesis and Translational Research (Ministry of Education), Department of Biochemistry and Molecular Biology, Peking University Cancer Hospital and Institute, Beijing, China. [2]State Key Laboratory of Natural and Biomimetic Drugs, School of Pharmaceutical Sciences, Peking University, Beijing, China. [3]Department of Pharmaceutical Science, Beijing Hospital, Beijing, China. [4]Key laboratory of Fertility Preservation and Maintenance of Ministry of Education, Department of Biochemistry and Molecular Biology, Ningxia Medical University, Yinchuan, China.

Note: Supplementary data for this article are available at Cancer Prevention Research Online (http://cancerprevres.aacrjournals.org/).

Corresponding Authors: Chengchao Shou, Peking University Cancer Hospital and Institute, 52 Fucheng Road, Beijing 100142, China. Phone: 86-10-8819-6766; Fax: 86-10-8812-2437; E-mail: scc@bjcancer.org; and Like Qu, qulike@bjcancer.org

doi: 10.1158/1940-6207.CAPR-14-0372

bioactive constituents of SW. The anticancer effect of SW fraction was further validated through *in vitro* and *in vivo* experiments. We demonstrated SW-induced cancer cell growth inhibition is partly associated with S phase arrest, apoptosis and autophagy through activation of the ERK1/2 pathway in a GSH/GSSG imbalance-dependent manner.

Materials and Methods

Materials and reagents

3-(4,5-dimethylthiazol-2-yl)-2,5-diphenyltetrazolium (MTT), crystal violet, DMSO, N-acetylcysteine (NAC), L-glutathione reduced (GSH), catalase, 3-methyladenine (3MA), BSA, RNase A, propidium iodide (PI), 4′,6-Diamidino-2-phenylindole (DAPI), PD98059, and nocodazole were purchased from Sigma-Aldrich. 5′-Bromo-2′-deoxyuridine (BrdUrd) and protease inhibitor cocktail were from Roche. Cyclophosphamide (CTX) was from Jiangsu Hengrui Medicine (Lianyungang, China). Antibodies against phospho-ERK1/2 (Thr202/Tyr204) and ERK1/2 were from Santa Cruz Biotechnology. Anti-BrdUrd antibody (clone 3D4) was from BD Biosciences. Anti-LC3 antibody (NB100-2220) for Western blot analysis was from Novus. Anti-LC3 antibody (PM036) for immunofluorescence and immunohistochemistry was from MBL. Horseradish peroxidase–conjugated or fluorescent dye–labeled secondary antibodies were from ZSGB-Bio. L-NMMA was from Beyotime. U0126 was from Cell Signal Technology.

Preparation and characterization of supernatant fraction from sarsaparilla

Sarsaparilla was purchased from Ben Cao Fang Yuan Pharmaceutical. The procedure for preparation of total ethanol extract (ST) was described previously (7). A 20,000 g powdered sarsaparilla was extracted by ethanol to get 2,552 g ST (yield percentage: 12.76%). ST was resuspended in deionized water and then extracted successively by petroleum ether, ethyl acetate, and n-butanol (H_2O-saturated) to obtain petroleum ether-soluble (SP), ethyl acetate-soluble (SE), and n-butanol-soluble (SB) fractions (19). The remaining water-soluble (SWT) fraction were further separated into the supernatant (SW) and precipitant (SWP) fractions by ethanol extraction. The yield percentage of SW was 7.27%. Liquid chromatography/mass spectrometry–ion trap–time-of-flight (LC/MS-IT-TOF) system (Shimadzu, Japan) was used for analysis of the chemical constituents of SW. The acquired data were processed by Shimadzu LC/MS solution Version 3.36, Formula Predictor Version 1.01, and Accurate Mass Calculator software. All fractions were solvent free through solvent removal and lyophilization. The solvent for preparation of all fractions (stock) was 3% DMSO in PBS and concentration of DMSO in working solutions was less than 0.15%. All the SW used in our experiments was from the same batch of preparation.

Cell lines and cell culture

BGC-823, MGC-803, HeLa, and GES-1 cells were kindly provided by Dr. Dajun Deng (Peking University Cancer Hospital & Institute, Beijing, China). BICR cells were gifted by Dr. Zhiqian Zhang (Peking University Cancer Hospital & Institute, Beijing, China). MDA-MB-231 and MCF-7 cells were gifted by Dr. Zhihua Liu (Cancer Institute & Hospital, Chinese Academy of Medical Science, Beijing, China). Mice H22 hepatocarcinoma cells were purchased from Beijing Cowin Biotech. AGS, HT-29, HepG2, PC3, T24, EJ, H1299, and PG cells were obtained from the ATCC. All cells were cultured under recommended conditions. Culture media and FBS were from Invitrogen. All cell lines were authenticated by short tandem repeat profiling. *Mycoplasma* test was performed biweekly by qPCR amplification of *M. hyorhinis p37*, Hochest 33258 staining, and PCR amplification of the rRNA gene sequences of *Mycoplasma* with a kit from HD Biosciences.

Cell growth assay

SW's effect on cancer cell growth was assessed by MTT assay and colony formation assay as previously described (7). Alternatively, cell confluence rates were measured by a CloneSelect Imager system (Molecular Devices) every 24 hours.

Tumor xenograft and allograft assays

Animal experiments were approved by the Biomedical Ethical Committee of Peking University Cancer Hospital and Institute and performed along institutional animal welfare guidelines concordant with the U.S. guidelines (NIH Publication #85-23, revised in 1985). Female BALB/c nude mice and BALB/c mice aged 7 to 8 weeks (Vital River Laboratories) were housed under specific pathogen-free conditions. A total of 2×10^5 HT-29 cells, 1×10^6 MDA-MB-231 cells, or 2.5×10^6 H22 cells were injected s.c. in the right flank of each mouse. When tumor sizes reached 100 mm^3, mice were grouped randomly with 7 or 4 mice each and given by oral gavage with 72.7 mg SW (prepared in PBS; equaling to 1 g crude sarsaparilla) once a day. The tumor width (W) and length (L) was measured every 3 days. Two (for H22) or 3 (for HT-29 and MDA-MB-231) weeks later, all mice were sacrificed and solid tumors were harvested, weighed, and pictured; tumor volume = $(W^2L)/2$.

Western blot and densitometric analyses

Cells were harvested in lysis buffer containing 50 mmol/L Tris-HCl pH7.0, 150 mmol/L NaCl, 2 mmol/L EDTA, 1% SDS, 2 mmol/L Dithiothreitol (DTT), and 1× protease inhibitor cocktail. The rest procedures were described previously (7). For quantification, the exposed films were scanned at the resolution of 600 dpi and analyzed by Image Pro Plus software. The optical density of each image was calibrated using "measure-calibration-intensity" command, and then the protein bands were selected out using "AOI" tool. The integrated optical density (IOD) value of each band was read out by the "Count/Size" tool.

Cell-cycle distribution assay

Cells were harvested by trypsinization following exposure to SW, and fixed in 75% ethanol at −20°C overnight. After being treated with RNase A for 30 minutes, cells were stained with PI and then analyzed by a FACS Calibur system (Becton Dickenson) with ModFit LT 3.0 (Verity Software House Inc.).

Cell synchronization

Subconfluent cells were synchronized at G_2–M phase by treatment with nocodazole (AGS: 30 ng/mL for 16 hours; HT-29: 200 ng/mL for 28 hours) in complete culture medium. At the end of treatment, conditioned medium were removed and replaced by fresh medium, cells were allowed to attach for 8 hours before exposure to SW.

BrdUrd–PI dual staining

Following exposure to SW for 24 hours, synchronized cells were pulse labeled with 10 μmol/L BrdUrd at 37°C for 1 hour, then

collected and fixed in 75% ethanol at −20°C overnight. After denaturing DNA with 2 N HCl and neutralizing with 0.1 mol/L sodium borate, cells were incubated with anti-BrdUrd antibody and subsequently FITC-conjugated secondary antibody at room temperature for 20 minutes. The samples were resuspended in PI staining solution before passing through FACS Calibur analyzer.

Immunofluorescence assay

Following treatment with SW, cells seeded on glass coverslips were fixed with prechilled 4% polyformaldehyde solution for 20 minutes and then permeabilized with 0.1% Triton X-100 in PBS for 5 minutes. Slides were incubated with anti-LC3 (1:200) at 4°C overnight and subsequently with FITC-labeled secondary antibody at room temperature for 45 minutes. Nuclei were counterstained with DAPI and images were captured by Leica TCS SP5 laser confocal microscope.

Immunohistochemistry

Paraffin-embedded HT-29 and MDA-MB-231 tumor sections were first deparaffinized with xylene twice for 15 minutes each, and then dehydrated with a gradient of ethanol (100%, 95%, 90%, 80%, and 70%) for 5 minutes each. After microwave treatment (500 W for 10 minutes) twice in 10 mmol/L citrate buffer (pH 6.3), slides were covered with 3% H_2O_2 for 10 minutes to block endogenous peroxidase activity. Next, slides were incubated with anti-LC3 primary antibody (1:1000 in 10% goat serum/PBS) at 4°C overnight and then visualized by EnVision Detection System (Dako).

GSH/GSSG ratio assay

Intracellular-reduced GSH and oxidized GSH (GSSG) were determined using modified Tietze recycling method (GSH and GSSG Assay Kit; Beyotime). Briefly, cells treated with SW or solvent were firstly collected through trypsinization and then lysed in ice-cold M buffer (containing sulfosalicylic acid, which inhibits γ-glutamyl transferase activity, thus preventing loss of GSH) by three freeze–thaw cycles. Cell lysate was kept on ice for 5 minutes before centrifugation at 10,000 × *g* at 4°C for 10 minutes. The supernatant was used directly for GSH determination but for GSSG determination, the supernatant required 2-vinylpyridine and triethanolamine treatment to remove existing GSH before running into following same steps as GSH determination. Standard curves of GSH and GSSG were made in each experiment for OD-to-concentration conversion.

ROS and NO measurement

Intracellular ROS and NO levels were evaluated using DCFH-DA and DAF-FM DA probes, respectively (Beyotime).

Annexin V–PI dual staining

The effect of SW on cell apoptosis was evaluated using the Annexin V–PI Dual Staining Assay Kit (Biosea).

Microarray analysis and real-time RT-PCR

RNA was extracted from solvent and SW-treated AGS cells with TRIzol reagent (Invitrogen). Gene-expression profiles were examined by ShangHai Biotech using Affymetrix Human Gene 1.0st microarrays containing 36,079 transcripts and variants. After normalization, the fold change was calculated. A *P* value of <0.05 and the fold change >1.5 were considered to be statistically significant. Microarray data can be tracked in NCBI Gene Expression Omnibus under accession no. GSE56593. Real-time RT-PCR was performed according to the manufacturer's instructions (SYBR, TOYOBO). The primers were listed in Supplementary Table S1.

Statistical analysis

Values represented the mean ± SD of at least two independent experiments. *P* values were calculated by the two-tailed Student *t* test or one-way ANOVA using IBM SPSS 18.0. A *P* value of less than 0.05 was considered statistically significant; */#, $P < 0.05$; **/##, $P < 0.01$; ***, $P < 0.001$.

Results

LC/MS-IT-TOF analysis of chemical constituents of SW fraction

We sequentially separated the total ethanol extract of sarsaparilla (ST) into petroleum ether-soluble (SP), ethyl acetate-soluble (SE), n-butanol-soluble (SB), and water-soluble (SWT) fractions as previously described (19). The SWTs were further divided into the supernatant (SW) and precipitant (SWP) fractions (Supplementary Fig. S1A). Through *in vitro* MTT assay with MCF-7 breast cancer and BGC-823 gastric cancer cells and IC_{50} measurement, we found the anticancer activity of SW was similar to that of ST and was higher than those of other five fractions (Supplementary Fig. S1B and S1C). The chemical composition of SW fraction was analyzed by the LC/MS-IT-TOF system. Besides bioactive flavonoids and phenylpropanoids reported in sarsaparilla, such as catechin (19), astilbin (18, 19), isoastilbin (18, 19), taxifolin (19), and smiglasides (20), we, for the first time, found 14 alkanoids in SW fraction (Fig. 1A and B).

SW fraction possesses anticancer effect

Because SW and ST showed similar effects, to minimize potential interferences from SP, SB, SE, or SWP fraction, next we focused on the effect of SW on cell growth by using 15 cell lines from different tissues. We found SW showed significant growth inhibition on cancer cell lines of gastric, lung, colon, bladder, breast, liver, prostate, and cervix origins, while exhibiting little toxicity to normal gastric epithelial cell line GES-1, suggesting a cancer-specific function of SW (Fig. 1C; Supplementary Fig. S2A). Results of colony formation assay confirmed SW's inhibition on the growth of seven cancer cell lines (Supplementary Fig. S2B). To evaluate SW's anticancer activity *in vivo*, we used tumor-bearing mice models. Oral administration of SW for 21 or 14 consecutive days significantly decreased the growth of HT-29 and MDA-MB-231 xenografts in BALB/c nude mice and H22 allografts in BALB/c mice (Fig. 1D and E; Supplementary Fig. S3A). These data revealed the anticancer potency of SW *in vitro* and *in vivo*.

SW fraction induces S phase arrest, apoptosis, and autophagy

Cell growth inhibition can be attributed to a block in cell-cycle progression or/and an increase in cell death (21). SW treatment resulted in increased S phase fraction in unsynchronized AGS and HT-29 cells, whereas no cell-cycle arrest was detected in MDA-MB-231 cells (Supplementary Fig. S3B). S phase arrest was also observed in synchronized AGS and HT-29 cells, with a concomitant decline in G_0–G_1 populations (Fig. 2A and B). Next, we found AGS and MDA-MB-231 cells underwent apoptosis after SW treatment; however, no apoptosis was induced in HT-29 cells (Fig. 2C; Supplementary Fig. S3C and 3D), suggesting a cell lineage

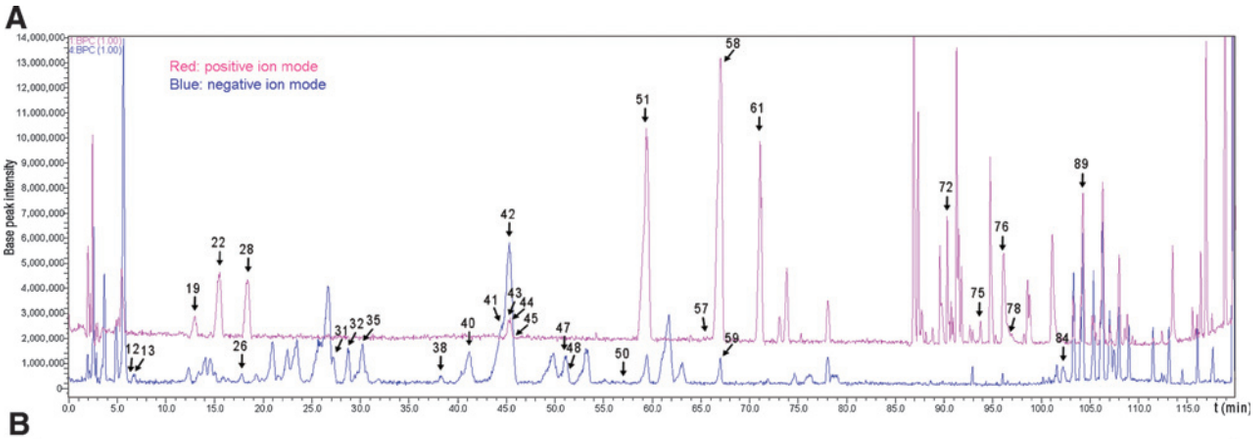

B

Major types	Compounds
Flavonoids	Catechin (26), (2S, 3S)-glucodistylin (35), Cinchonainla (38), Astilbin (40), Isoastilbin (41), Neoastilbin (42), Taxfolin (43), Neoisoastilbin (47), Quercetin-3-O-α-L-rhamnoside (50), Engelitin (51), Quercetin-4'-O-β-D-glucoside (57), Cinchonain Ib (61)
Alkaloids	12, 13,19, 22, 27, 28, 32, 44, 45, 58, 59, 72, 84, 89
Phenylpropanoids	Cassiamin A (31), Cassiamin B (48), Smiglaside E (75), Smiglaside A (78)

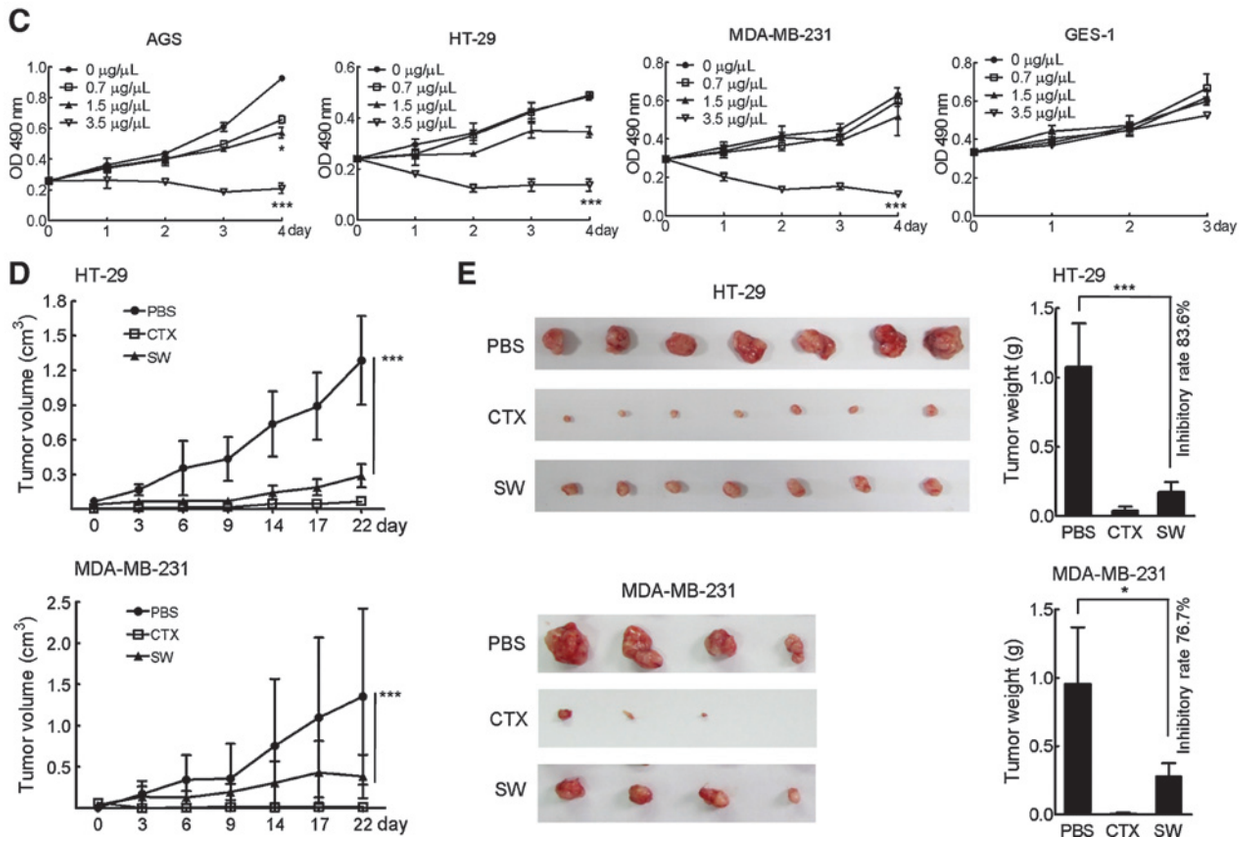

Figure 1.
SW fraction inhibits cancer cell growth *in vitro* and *in vivo*. A, base peak chromatograms (BPC) of SW. The characterized chemical compounds were indicated with numbered arrows. Red, positive ion mode; blue, negative ion mode. B, categorization of the numbered chemical compounds in A. C, cell growth curve of AGS, HT-29, MDA-MB-231, and GES-1 cells in response to SW, as monitored by MTT assay. Composite results from three independent experiments with triplicate wells were shown. D, tumor growth graphs of HT-29 ($n = 7$) and MDA-MB-231 ($n = 4$) xenografts in mice administrated with PBS, CTX (80 mg/kg once a week) and SW (72.7 mg once a day). CTX, cyclophosphamide, positive control. E, left, pictures of HT-29 and MDA-MB-231 xenografts. Right, quantification of tumor weights. Columns, mean; bars, SD. *, $P < 0.05$; ***, $P < 0.001$.

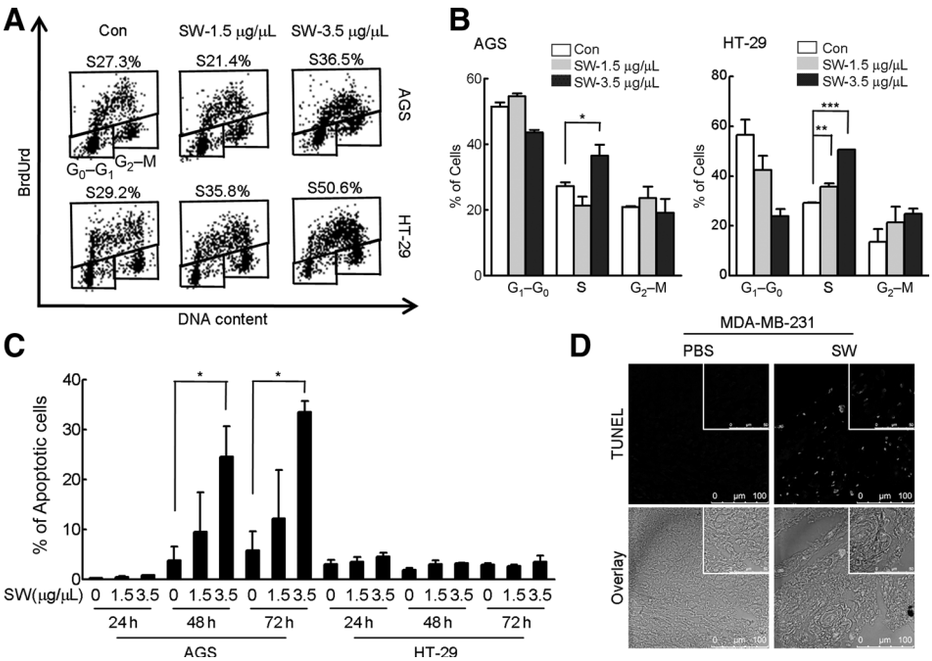

Figure 2.
SW fraction induces S phase arrest and apoptosis. A, BrdUrd–PI labeling of synchronized AGS and HT-29 cells treated with SW or solvent for 24 hours. BrdUrd-positive cells were determined as S phase fraction and shown as the percentage. Results from one representative experiment were shown. B, composite results of two BrdUrd–PI labeling experiments with duplicate samples. Columns, mean; bars, SD. C, annexin V–PI staining of AGS and HT-29 cells treated with SW. Percentages of apoptotic cells were shown by composite results of two experiments with duplicate samples. Columns, mean; bars, SD. D, TUNEL staining of paraffin-embedded MDA-MB-231 xenograft sections; scale bar, 100 μm. *, $P < 0.05$; **, $P < 0.01$; ***, $P < 0.001$.

specificity of SW on apoptosis. Results of TUNEL assay further verified the presence of apoptosis in SW-treated MDA-MB-231 xenografts (Fig. 2D). LC3II, a marker of autophagy (22), was upregulated in SW-treated AGS and HT-29 cells, although with different kinetics (Fig. 3A). Immunostaining of LC3II confirmed the autophagosome formation in SW-treated AGS, HT-29, and MDA-MB-321 cells (Fig. 3B and Supplementary Fig. S3D), which was abolished by pretreatment of autophagy-specific inhibitor 3MA (Fig. 3B). Furthermore, autophagy was induced in SW-treated HT-29 and MDA-MB-231 xenografts (Fig. 3C), thus confirming the proautophagic function of SW *in vivo*. In addition, pan-caspase inhibitor z-VAD-FMK, instead of 3MA, partly antagonized SW-induced growth inhibition in AGS cells, whereas in HT-29 cells, 3MA, instead of z-VAD-FMK, showed a partially reversal effect on SW-induced growth inhibition (Fig. 3D and E). Therefore, contributions of apoptotic death and autophagic death to SW-induced growth inhibition are cell type dependent.

GSH/GSSG imbalance accounts for SW-induced S phase arrest, apoptosis, autophagy, and cell growth inhibition

Previously, we performed gene microarray screening with RNA samples from ST fraction-treated MCF-7 and HT-29 cells and found that the expressions of genes involved in proliferation, cell cycle, apoptosis, oxidative stress, and MAPK signaling were significantly affected by sarsaparilla (7). In this study, we performed gene-expression profiling assay with RNA samples from SW-treated AGS cells. Analysis of all differentially expressed genes revealed a cluster of oxidative stress-related genes (Fig. 4A), which were validated by quantitative RT-PCR assay (Fig. 4B). Among oxidative stress-related genes, *GCLC*, *GCLM*, *GPX5*, *GPX2*, and *G6PD* have been implicated in GSH metabolism (23); therefore, we evaluated the intercellular reduced glutathione/oxidized glutathione (GSH/GSSG) ratio, one hallmark of oxidative stress (24). We found AGS and HT-29 cells suffered a marked GSH/GSSG imbalance following SW treatment for 0.5 and 24 hours (Fig. 4C). NAC, which could enrich intracellular GSH pool (25), restored SW-induced GSH/GSSG imbalance (Fig. 4C). Moreover, GSH or NAC partially reversed SW-induced S phase arrest, apoptosis, autophagy, and cell growth inhibition in AGS and HT-29 cells (Fig. 4D–G), underlining the importance of GSH/GSSG imbalance in mediating SW's anticancer effect. Next, we examined another two hallmarks of oxidative stress, that is, reactive oxygen species (ROS) and nitric oxide (NO). Little alteration in ROS production was detected in SW-treated cells (Supplementary Fig. S4A). ROS inhibitor catalase, which eliminates H_2O_2, exerted no reversing effect on SW-induced S phase accumulation or growth inhibition (Supplementary Fig. S4B and S4C), thus excluding the possible involvement of ROS in SW-induced oxidative stress. As for NO, we observed increased NO levels at 3 hours after SW treatment in AGS and HT-29 cells (Supplementary Fig. S4D). However, pan-inhibitor of NO synthase L-NMMA could not abrogate SW-induced S phase accumulation or growth inhibition (Supplementary Fig. S4E and F). These results suggested that oxidative stress, resulting from GSH/GSSG imbalance rather than increased H_2O_2 or NO, was responsible for SW-induced S phase arrest, apoptosis, autophagy, and growth inhibition.

GSH/GSSG imbalance-induced ERK1/2 phosphorylation contributes to SW-induced S phase arrest, apoptosis, autophagy, and growth inhibition

Results of microarray assay suggested that the MAPK1 signaling pathway was also potentially associated with SW treatment (Fig. 4A), which was in agreement with our previous finding (7). We noticed that ERK1/2 phosphorylation was induced at 30 minutes after SW treatment and sustained for 24 hours (Fig. 5A). In addition, it exhibited a redox-dependent manner, as both NAC and GSH remarkably abolished SW-induced ERK1/2 phosphorylation (Fig. 5B). SW-induced ERK1/2 phosphorylation could be lowered by pretreatment with MAPK kinase inhibitor U0126 (Supplementary Fig. S5A), but U0126 could not reverse

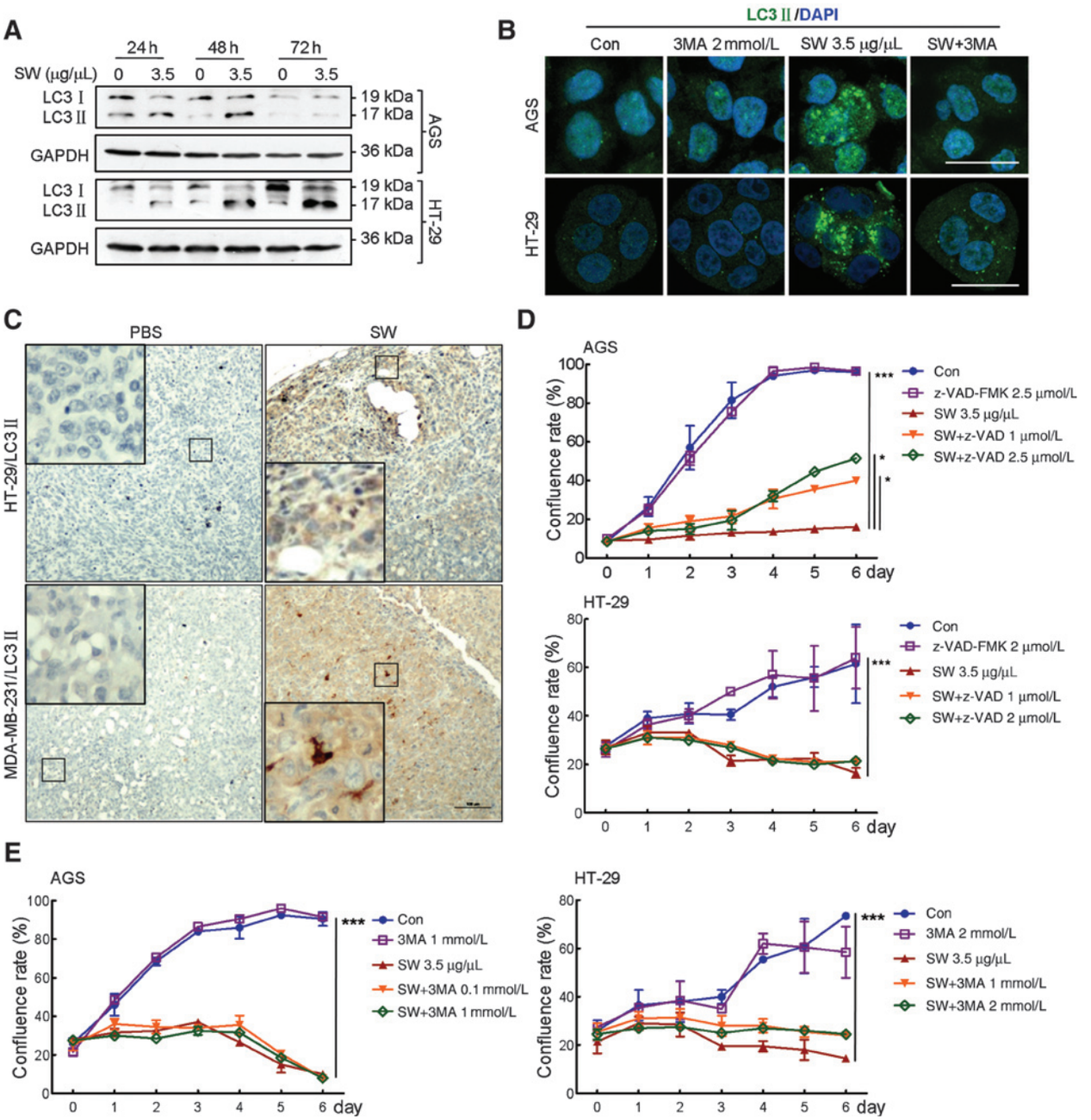

Figure 3.
SW fraction induces autophagy. A, cleavages of LC3 in SW-treated AGS and HT-29 cells. B, autophagosome formation in cells treated with SW, 3MA, and both; scale bars, 50 μm in AGS cells and 25 μm in HT-29 cells. C, immunohistochemical staining of LC3 in paraffin-embedded HT-29 and MDA-MB-231 tumor sections; scale bar, 100 μm. D and E, the effects of z-VAD-FMK (D) and 3MA (E) on SW-induced growth inhibition in AGS and HT-29 cells. Cell confluence rates were shown by composite results of two experiments with duplicate samples. *, $P < 0.05$; ***, $P < 0.001$.

SW-induced GSH/GSSG imbalance (Supplementary Fig. S5B), implying that ERK1/2 phosphorylation was not upstream of deregulated GSH/GSSG in the context of SW treatment. Following pretreatment with U0126 or/and PD98059, SW-induced S phase arrest, apoptosis, autophagy, and resultant growth inhibition were partially antagonized (Fig. 6A–D). These results support the notion that SW triggers ERK1/2 phosphorylation in a GSH/GSSG imbalance-dependent fashion, thereby causing S phase arrest, apoptosis, autophagy, and cell growth inhibition (Fig. 6E).

Discussion

Besides as a natural dietary supplement, sarsaparilla has been used to treat cancer in Southeast Asia (15, 17, 26, 27). To

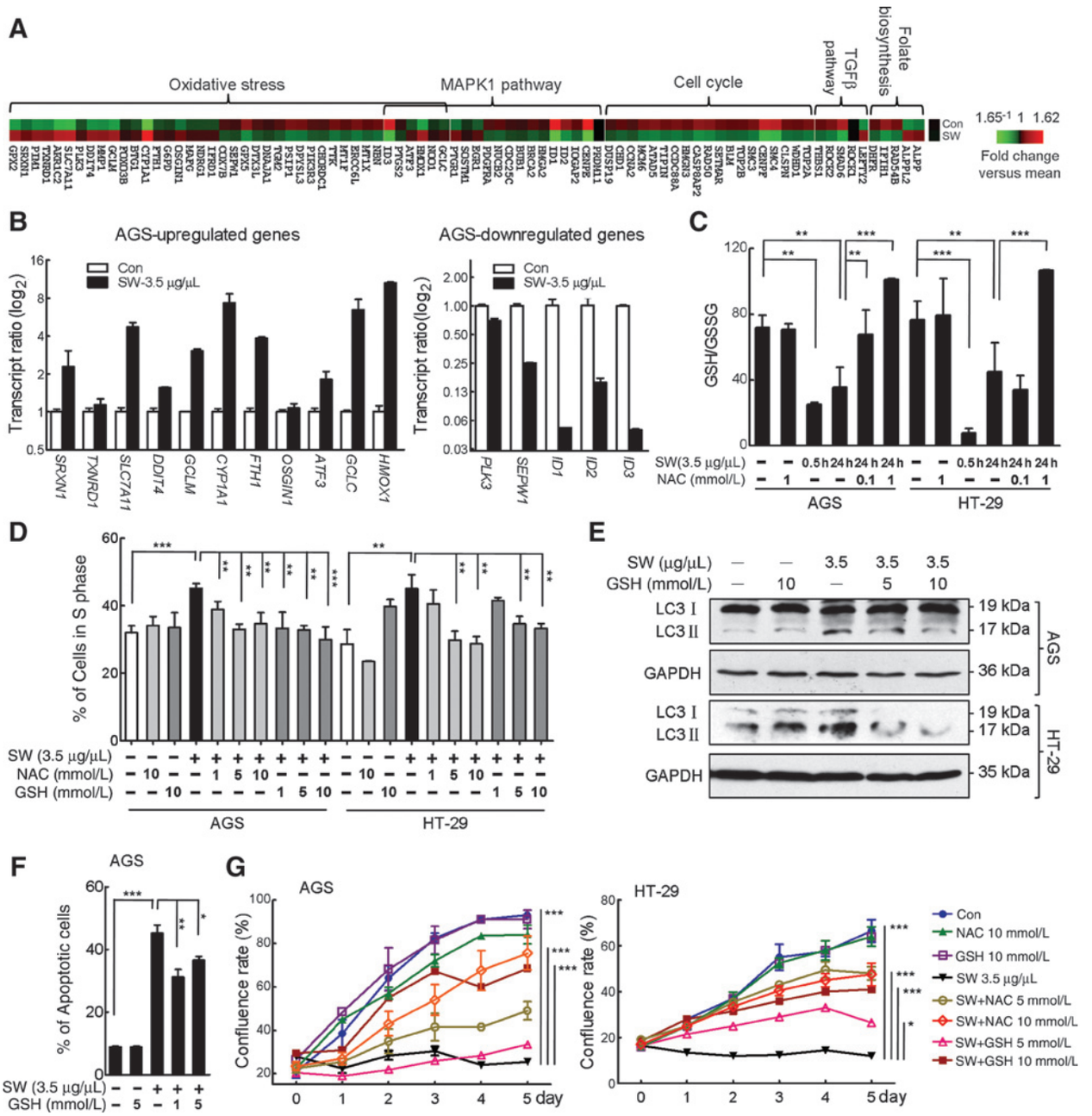

Figure 4.
GSH/GSSG imbalance is associated with SW-induced S phase arrest, apoptosis, autophagy, and cancer cell growth inhibition. A, KEGG database was used to analyze the pathways possibly involved in the SW-induced biologic processes. Pathways with *P* value (genelist vs. pathways comparison similarity) < 0.05 and *q* value (confidence of the pathway) < 0.05 were considered to be statistically significant. B, real-time RT-PCR verification of a subset of genes related to oxidative stress and MAPK pathway in AGS cells treated with SW. C, the GSH/GSSG ratio. Cells were pretreated with NAC for 2 hours before exposure to SW. Columns, mean; bars, SD. D and G, the effects of NAC and GSH on SW-induced S phase accumulation (D) and growth inhibition (G). The percentages of S phase population and cell confluence rates were composite results of two experiments with duplicate samples. E and F, the effects of GSH on SW-induced cleavage of LC3 (E) and SW-promoted apoptosis (F) in AGS or/and HT-29 cells. Percentages of apoptotic cells were shown as composite results of two experiments with duplicate samples. Columns, mean; bars, SD. *, $P < 0.05$; **, $P < 0.01$; ***, $P < 0.001$.

date, several compounds were isolated from sarsaparilla and shown to possess certain anticancer potency, such as apigenin (28), astilbin (19, 29), taxifolin (19, 30), neoastilbin (19), isoastilbin (19), neoisoastilbin (19), and engelitin (31). In this study, we found SW fraction had strongest anticancer activity among the six fractions sequentially extracted from total extract (ST) of sarsaparilla. Because ST and SW had similar IC_{50} values, it would be cost-effective and easier to use ST for treatment of cancer.

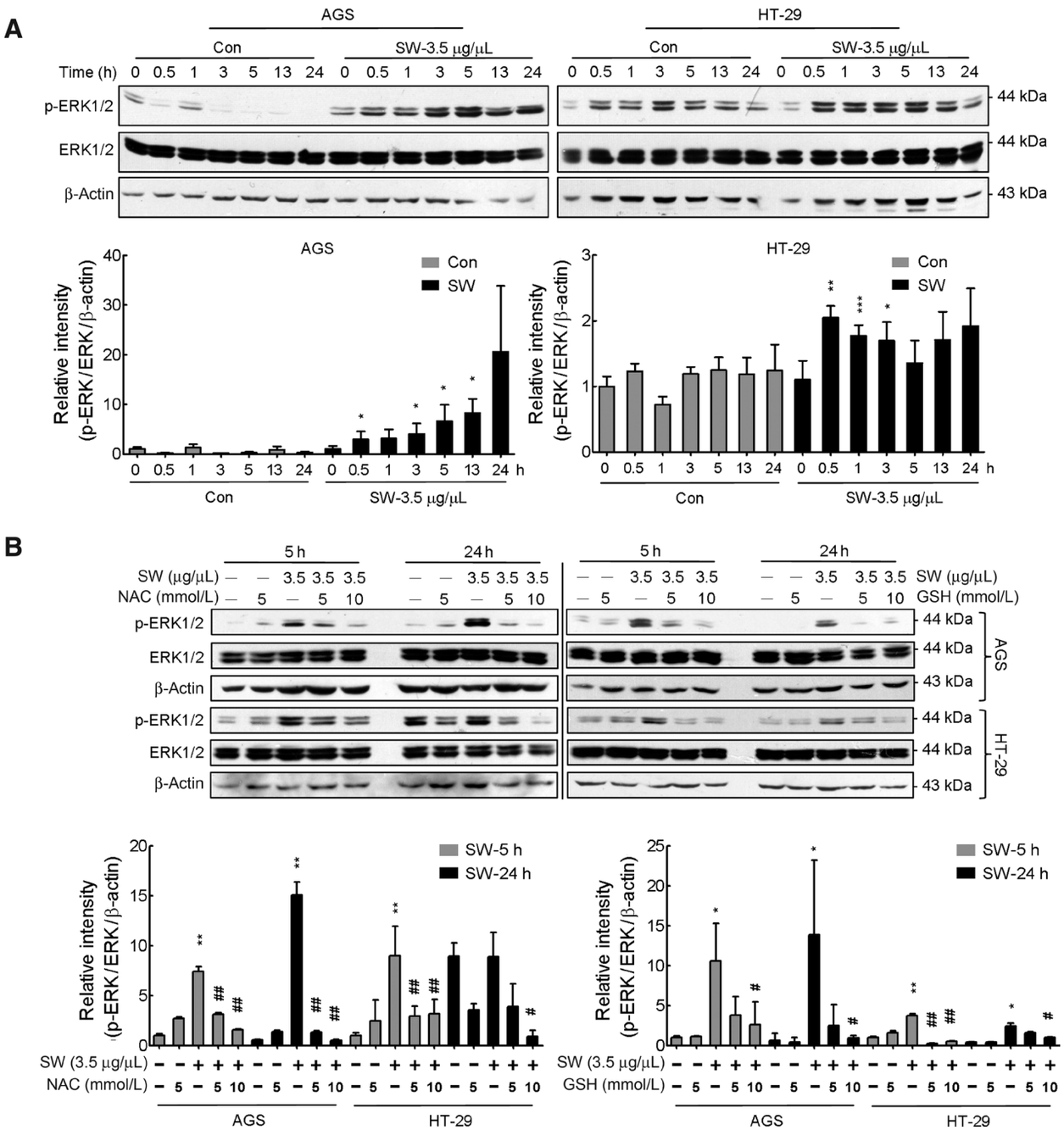

Figure 5.

SW fraction activates the ERK1/2 pathway in a GSH/GSSG imbalance–dependent manner. A, top, representative immunoblotting pictures of ERK1/2 phosphorylation induced by SW in AGS and HT-29 cells. Bottom, relative intensity graphs resulted from composite results of three independent experiments. The phosphorylation level of ERK1/2 was calculated by the formula p-ERK/ERK/β-actin. The values obtained were then divided by the 0 hours (control) value to get the relative i ntensity values. B, top, representative immumoblotting pictures showing the effects of NAC and GSH on SW-induced ERK1/2 phosphorylation. Bottom, relative intensity graphs resulted from two independent experiments. The measure for testing p-ERK levels was the same as in A, and the relative intensity values were obtained by the p-ERK value divided by corresponding 5 or 24 hours control counterpart. *, the statistically significant difference between control and SW-treated groups; #, the statistically significant difference between SW-treated and SW-plus-NAC/GSH–treated groups. */#, $P < 0.05$; **/##, $P < 0.01$; ***, $P < 0.001$.

Through LC/MS-IT-TOF analysis of SW fraction, several above-mentioned compounds such as astilbin and taxifolin were also identified in SW. Interestingly, alkaloids were newly identified from sarsaparilla, possibly due to our modified extraction method. Therefore, the anticancer effect of SW might be determined by the combined action of multiple compounds in the mixture. The characterization of SW-derived alkaloids and their contributions to sarsaparilla's biologic effects are still in progress. Moreover, two

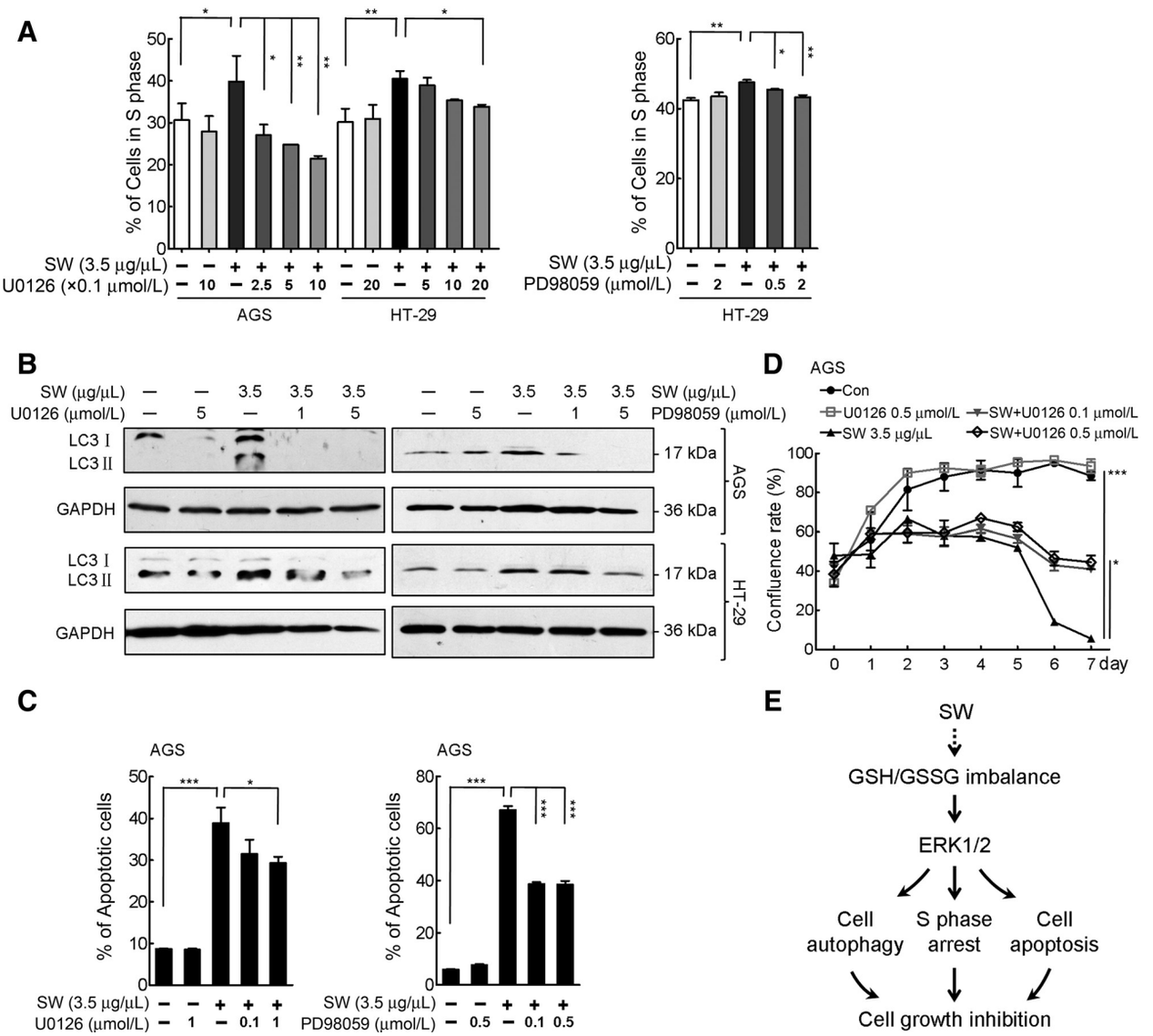

Figure 6.

ERK1/2 phosphorylation associates with SW-induced S phase arrest, apoptosis, autophagy, and growth inhibition. A, BrdU–PI labeling of S phase in AGS and HT-29 cells treated with SW plus U0126 or PD98059. Composite results of two experiments with duplicate samples were shown. Columns, mean; bars, SD. B and C, the effects of U0126 and PD98059 on SW-induced cleavage of LC3 (B) and SW-promoted apoptosis (C) in AGS or/and HT-29 cells. Percentages of apoptotic cells were shown by composite results of two experiments with duplicate samples. Columns, mean; bars, SD. D, the effect of U0126 on SW-induced growth inhibition in AGS cells. Cell confluence rates were composite results of two experiments with duplicate samples. E, signaling events mediating SW-induced cancer cell growth inhibition. *, $P < 0.05$; **, $P < 0.01$; ***, $P < 0.001$.

constituents from SW, taxifolin, and apigenin, were shown to have chemopreventive functions (28, 30), underlying the possible role of sarsaparilla in cancer prevention.

In addition to previously reported S phase arrest and apoptosis (7, 18), we, for the first time, found the proautophagic function of sarsaparilla. Both prosurvival and antisurvival functions of autophagy have been demonstrated (22, 32, 33). The role of autophagy in oxidative stress-induced cell death depends on cell type (34, 35). In our study, SW induced autophagy in AGS, HT-29, and MDA-MB-231 cells, but apoptosis was not found in HT-29 cells. Meanwhile, only z-VAD-FMK could partly reversed SW-induced cell growth inhibition in AGS cells whereas in HT-29 cells only 3MA could do. Such cell lineage specificity has been noticed previously. For instance, triptolide-treated MiaPaCa-2 cells underwent apoptosis, whereas triptolide-treated S2-013 and S2-VP10 cells went for autophagy-related cell death, despite they are all pancreatic cancer cells (21). In addition, c-Jun NH2-terminal kinase inhibitor SP600125 could inhibit the proliferation of both AGS and HT-29 cells, with apoptosis only induced in AGS cells, possible due to the difference in the basal levels of JNK2 (36). Comparison of pathways targeted by SW in different cells will provide explanation for the disparity in death response.

Bioactive compounds of sarsaparilla, such as astilbin and taxifolin, were shown to inhibit oxidative stress (37, 38), whereas ST fraction increased ROS production (7). Here, we found no ROS was induced by SW. The different effects on oxidative stress might be attributed to the integrated functions of distinct compositions. The GSH/GSSG ratio, as a crucial determinant of intercellular redox status (24), was deregulated in SW-treated AGS and HT-29 cells. Supplement with NAC or GSH abrogated SW-induced S phase arrest, apoptosis, autophagy, and resultant cell growth inhibition, underscoring the crucial role of GSH in sarsaparilla's anticancer effect. Decline in antioxidants and/or boost in other oxidative signals than H_2O_2 or NO might play some roles, which deserves further exploration. Increased transcription of GSH synthesis-related genes, such as *GCLM*, *GCLC*, and *G6PD* (23), did not restore GSH/GSSH balance, suggesting that these changes were likely the adaptive response to SW treatment.

Metabolism-targeted therapy shows great potential and advantage in cancer treatment (39). Chemicals targeting the enzymes essential for cancer metabolism, such as pyruvate kinase M2 (40), pyruvate dehydrogenase kinase (PDK; ref. 41) and lactate dehydrogenase (39), are currently tested in preclinical or clinical trials. Dichloroacetate, an orally available inhibitor of PDK, was found to promote the apoptosis of cancer cells in multiple *in vitro* and *in vivo* models (41). Normal cells, however, were unaffected by dichloroacetate, perhaps due to low level of PDK activity (41). Our results indicated that SW affected the expression of many metabolism-related genes. It is likely that SW might target some metabolic pathways that are necessary for the survival of cancer cells, but dispensable for the normal cells, thus leading to the preference of SW for cancer cells. However, which pathways were majorly targeted and how they were disrupted by SW are still under investigation.

ERK has been deemed as a therapeutical target because of its antiapoptotic function in cancer cells (42), but context-dependent proapoptotic effect of ERK was also documented. Redox-triggered ERK1/2 phosphorylation could induce both intrinsic and extrinsic apoptotic pathways (43, 44), and autophagy can be positively regulated by ERK1/2 (21). Various drugs induced autophagies were correlated with a persistent activation or cytoplasmic sequestration of ERK1/2 (21, 45). Furthermore, Selenomethionine, an anticancer agent already used in clinical trials, could induce sustained phosphorylation of ERK and S/G_2–M phase arrest in HCT116 and SW48 cells (46). In the present study, we observed a sustained phophorylation of ERK in SW-treated AGS and HT-29 cells. Meanwhile, U0126 or/and PD98059 antagonized SW-induced effects, highlighting ERK as a critical target of sarsaparilla.

Together, we demonstrated the anticancer effect of SW over multiple cell lines *in vitro and in vivo*, which was associated with S phase arrest, autophagy, and apoptosis. Moreover, we uncovered a GSH/GSSG imbalance-dependent activation of the ERK1/2 pathway in SW-treated cells, which was responsible for the anticancer effect of SW fraction (Fig. 6E). Our results suggest sarsaparilla, as a potential anticancer agent, shows great promise in future preclinical and clinical applications.

Disclosure of Potential Conflicts of Interest

No potential conflicts of interest were disclosed.

Authors' Contributions

Conception and design: T. She, L. Qu, C. Shou
Development of methodology: T. She, S. Cai
Acquisition of data (provided animals, acquired and managed patients, provided facilities, etc.): T. She, L. Wang, X. Yang, S. Xu, J. Feng, Y. Gao
Analysis and interpretation of data (e.g., statistical analysis, biostatistics, computational analysis): T. She, L. Qu, C. Zhao, Y. Han
Writing, review, and/or revision of the manuscript: T. She, L. Qu
Administrative, technical, or material support (i.e., reporting or organizing data, constructing databases): L. Wang, X. Yang, S. Xu, J. Feng, C. Zhao, S. Cai
Study supervision: L. Qu, Y. Han, C. Shou

Acknowledgments

The authors deeply appreciate Dr. Dajun Deng (Peking University Cancer Hospital and Institute), Dr. Zhiqian Zhang (Peking University Cancer Hospital and Institute), and Dr. Zhihua Liu (Cancer Institute and Hospital, Chinese Academy of Medical Science) for providing the cell lines.

Grant Support

This work was supported by the National Basic Research Program of China (2015CB553906; to C. Shou and 2013CB910504; to L. Qu).

The costs of publication of this article were defrayed in part by the payment of page charges. This article must therefore be hereby marked *advertisement* in accordance with 18 U.S.C. Section 1734 solely to indicate this fact.

Received October 22, 2014; revised January 29, 2015; accepted February 10, 2015; published OnlineFirst March 2, 2015.

References

1. Ferlay J, Shin HR, Bray F, Forman D, Mathers C, Parkin DM. Estimates of worldwide burden of cancer in 2008: GLOBOCAN 2008. Int J Cancer 2010;127:2893–917.
2. Cassileth BR, Vickers AJ. High prevalence of complementary and alternative medicine use among cancer patients: implications for research and clinical care. J Clin Oncol 2005;23:2590–2.
3. Wieland LS, Manheimer E, Berman BM. Development and classification of an operational definition of complementary and alternative medicine for the Cochrane collaboration. Altern Ther Health Med 2011;17:50–9.
4. Cam.Cancer.gov [Internet]. Rockville: Office of Cancer Complementary and Alternative Medicine (OCCAM) National Cancer Institute, NIH; c1998–2011 [updated 2013 Aug 2; cited 2014 Sept 24]. Available from: http://cam.cancer.gov/cam_annual_report_fy11.pdf.
5. Ray RB, Raychoudhuri A, Steele R, Nerurkar P. Bitter melon (Momordica charantia) extract inhibits breast cancer cell proliferation by modulating cell cycle regulatory genes and promotes apoptosis. Cancer Res 2010;70:1925–31.
6. Wu Q, Kohli M, Bergen HR III, Cheville JC, Karnes RJ, Cao H, et al. Preclinical evaluation of the supercritical extract of azadirachta indica (neem) leaves *in vitro* and *in vivo* on inhibition of prostate cancer tumor growth. Mol Cancer Ther 2014;13:1067–77.
7. Gao Y, Su Y, Qu L, Xu S, Meng L, Cai SQ, et al. Mitochondrial apoptosis contributes to the anti-cancer effect of Smilax glabra Roxb. Toxicol Lett 2011;207:112–20.
8. Foods, Herbs & Supplements [Internet]. Somerville: Natural Standard; c2001–2014 [cited 2013 Aug 18]. Available from: http://www.naturalstandard.com/databases/herbssupplements/all/a/.
9. Galhena PB, Samarakoon SR, Thabrew MI, Weerasinghe GA, Thammitiyagodage MG, Ratnasooriya WD, et al. Anti-inflammatory activity is a possible mechanism by which the polyherbal formulation comprised of Nigella sativa (seeds), Hemidesmus indicus (root), and Smilax glabra (rhizome) mediates its antihepatocarcinogenic effects. Evid Based Complement Alternat Med 2012;2012:108626.
10. Wang J, Li Q, Ivanochko G, Huang Y. Anticancer effect of extracts from a North American medicinal plant—wild sarsaparilla. Anticancer Res 2006;26:2157–64.
11. Tropical Plant Database [Ineternet]. Milam county: Rain Tree; c1996–2014 [updated 2012 Dec 29; cited 2013 Aug 24]. Available from: http://www.rain-tree.com/sarsaparilla.htm#.Uz-tenlPIu4.

12. Jiang J, Xu Q. Immunomodulatory activity of the aqueous extract from rhizome of Smilax glabra in the later phase of adjuvant-induced arthritis in rats. J Ethnopharmacol 2003;85:53–9.
13. Xu Q, Wu F, Cao J, Chen T, Jiang J, Saiki I, et al. Astilbin selectively induces dysfunction of liver-infiltrating cells—novel protection from liver damage. Eur J Pharmacol 1999;377:93–100.
14. Fukunaga T, Miura T, Furuta K, Kato A. Hypoglycemic effect of the rhizomes of Smilax glabra in normal and diabetic mice. Biol Pharm Bull 1997;20:44–6.
15. Iddamaldeniya SS, Thabrew MI, Wickramasinghe SM, Ratnatunge N, Thammitiyagodage MG. A long-term investigation of the anti-hepatocarcinogenic potential of an indigenous medicine comprised of Nigella sativa, Hemidesmus indicus and Smilax glabra. J Carcinog 2006;5:11.
16. Huang YG, Li QZ, Ivanochko G, Wang R. Novel selective cytotoxicity of wild sarsaparilla rhizome extract. J Pharm Pharmacol 2006;58: 1399–403.
17. Tian H, Li H, Wang B, Liang G, Huang X, Huang Z, et al. Treatment of middle/late stage primary hepatic carcinoma by Chinese medicine comprehensive therapy: a prospective randomized controlled study. Chin J Integr Med 2010;16:102–8.
18. Sa F, Gao JL, Fung KP, Zheng Y, Lee SM, Wang YT. Anti-proliferative and pro-apoptotic effect of Smilax glabra Roxb. extract on hepatoma cell lines. Chem Biol Interact 2008;171:1–14.
19. Xu S, Shang MY, Liu GX, Xu F, Wang X, Shou CC, et al. Chemical constituents from the rhizomes of Smilax glabra and their antimicrobial activity. Molecules 2013;18:5265–87.
20. Chen T, Li JX, Xu Q. Phenylpropanoid glycosides from Smilax glabra. Phytochemistry 2000;53:1051–5.
21. Mujumdar N, Mackenzie TN, Dudeja V, Chugh R, Antonoff MB, Borja-Cacho D, et al. Triptolide induces cell death in pancreatic cancer cells by apoptotic and autophagic pathways. Gastroenterology 2010;139: 598–608.
22. Sato K, Tsuchihara K, Fujii S, Sugiyama M, Goya T, Atomi Y, et al. Autophagy is activated in colorectal cancer cells and contributes to the tolerance to nutrient deprivation. Cancer Res 2007;67:9677–84.
23. Bentley AR, Emrani P, Cassano PA. Genetic variation and gene expression in antioxidant related enzymes and risk of COPD: a systematic review. Thorax 2008;63:956–61.
24. Menon SG, Goswami PC. A redox cycle within the cell cycle: ring in the old with the new. Oncogene 2007;26:1101–9.
25. Rahman I, MacNee W. Oxidative stress and regulation of glutathione in lung inflammation. Eur Respir J 2000;16:534–54.
26. Thabrew MI, Mitry RR, Morsy MA, Hughes RD. Cytotoxic effects of a decoction of Nigella sativa, Hemidesmus indicus and Smilax glabra on human hepatoma HepG2 cells. Life Sci 2005;77:1319–30.
27. Zhang Q, Zhang Z, Cheung H. Antioxidant activity of Rhizoma Smilacis Glabrae extracts and its key constituent-astilbin. Food Chem 2009; 115:297–303.
28. Patel D, Shukla S, Gupta S. Apigenin and cancer chemoprevention: progress, potential and promise (review). Int J Oncol 2007;30:233–45.
29. Yan R, Xu Q. Astilbin selectively facilitates the apoptosis of interleukin-2-dependent phytohemagglutinin-activated Jurkat cells. Pharmacol Res 2001;44:135–9.
30. Oi N, Chen H, Ok KM, Lubet RA, Bode AM, Dong Z. Taxifolin suppresses UV-induced skin carcinogenesis by targeting EGFR and PI3K. Cancer Prev Res 2012;5:1103–14.
31. Wu LS, Wang XJ, Wang H, Yang HW, Jia AQ, Ding Q. Cytotoxic polyphenols against breast tumor cell in Smilax china L. J Ethnopharmacol 2010;130:460–4.
32. Jin S, White E. Role of autophagy in cancer: management of metabolic stress. Autophagy 2007;3:28–31.
33. Codogno P, Meijer AJ. Autophagy and signaling: their role in cell survival and cell death. Cell Death Differ 2005;12:1509–18.
34. Scherz-Shouval R, Shvets E, Fass E, Shorer H, Gil L, Elazar Z. Reactive oxygen species are essential for autophagy and specifically regulate the activity of Atg4. EMBO J 2007;26:1749–60.
35. Azad MB, Chen Y, Gibson SB. Regulation of autophagy by reactive oxygen species (ROS): implications for cancer progression and treatment. Antioxid Redox Signal 2009;11:777–90.
36. Xia HH, He H, De Wang J, Gu Q, Lin MC, Zou B, Yu LF, Sun YW, Chan AO, Kung HF, Wong BC. Induction of apoptosis and cell cycle arrest by a specific c-Jun NH2-terminal kinase (JNK) inhibitor, SP-600125, in gastrointestinal cancers. Cancer Lett 2006;241:268–74.
37. Petacci F, Freitas SS, Brunetti IL, Khalil NM. Inhibition of peroxidase activity and scavenging of reactive oxygen species by astilbin isolated from Dimorphandra mollis (Fabaceae, Caesalpinioideae). Biol Res 2010;43:63–74.
38. Trouillasa P, Fagnère C, Lazzaroni R, Calliste C, Marfak A, Duroux J. A theoretical study of the conformational behavior and electronic structure of taxifolin correlated with the free radical-scavenging activity. Food Chem 2004;88:571–82.
39. Sanchez-Arago M, Formentini L, Cuezva JM. Mitochondria-mediated energy adaption in cancer: the H(+)-ATP synthase-geared switch of metabolism in human tumors. Antioxid Redox Signal 2013;19:285–98.
40. Anastasiou D, Yu Y, Israelsen WJ, Jiang JK, Boxer MB, Hong BS, et al. Pyruvate kinase M2 activators promote tetramer formation and suppress tumorigenesis. Nat Chem Biol 2012;8:839–47.
41. Bonnet S, Archer SL, Allalunis-Turner J, Haromy A, Beaulieu C, Thompson R, et al. A mitochondria-K^+ channel axis is suppressed in cancer and its normalization promotes apoptosis and inhibits cancer growth. Cancer Cell 2007;11:37–51.
42. Pratilas CA, Solit DB. Targeting the mitogen-activated protein kinase pathway: physiological feedback and drug response. Clin Cancer Res 2010;16:3329–34.
43. Lu TH, Tseng TJ, Su CC, Tang FC, Yen CC, Liu YY, et al. Arsenic induces reactive oxygen species-caused neuronal cell apoptosis through JNK/ERK-mediated mitochondria-dependent and GRP 78/CHOP-regulated pathways. Toxicol Lett 2014;224:130–40.
44. Lin KL, Su JC, Chien CM, Tseng CH, Chen YL, Chang LS, et al. Naphtho[1,2-b]furan-4,5-dione induces apoptosis and S-phase arrest of MDA-MB-231 cells through JNK and ERK signaling activation. Toxicol In Vitro 2010; 24:61–70.
45. Cagnol S, Chambard JC. ERK and cell death: mechanisms of ERK-induced cell death–apoptosis, autophagy and senescence. FEBS J 2010;277:2–21.
46. Goulet AC, Chigbrow M, Frisk P, Nelson MA. Selenomethionine induces sustained ERK phosphorylation leading to cell-cycle arrest in human colon cancer cells. Carcinogenesis 2005;26:109–17.